Journal of Hazardous Materials 213–214 (2012) 361–368

Contents lists available at SciVerse ScienceDirect

Journal of Hazardous Materials

journal homepage: www.elsevier.com/locate/jhazmat

Simple synthesis of Ni-containing ordered mesoporous carbons and their adsorption/desorption of methylene orange

Yong Tian, Xiufang Wang*, Yufang Pan

College of Pharmacy, Guangdong Pharmaceutical University, Guangzhou 510006, China

ARTICLE INFO

Article history:
Received 13 October 2011
Received in revised form 10 January 2012
Accepted 4 February 2012
Available online 13 February 2012

Keywords:
Mesoporous carbon
Nickel
Synthesis
Adsorption
Desorption

ABSTRACT

A simple route has been developed to synthesize magnetic Ni-containing ordered mesoporous carbons (Ni/OMCs) without using a solvent for dissolving carbon precursor or magnetic source. The adsorption and desorption of methylene orange (MO) on the obtained Ni/OMCs were investigated. The effects of $Ni(NO_3)_2$ loading amount and carbonization temperature on the morphologies, the structural parameters and magnetic properties of these Ni/OMCs were evaluated by X-ray diffraction(XRD), N_2 sorption analysis, transmission electron microscopy(TEM) and physical property measurements. With the increase of $Ni(NO_3)_2$ loading amount, the ordering of the mesoporous structures, the specific surface area and the total pore volumes of Ni/OMCs decreased, but the pore diameters of Ni/OMCs and the sizes of Ni particle increased. The saturation magnetization strength could be easily adjusted by varying the amount of $Ni(NO_3)_2$. The specific surface area and total pore volumes decreased with the increasing of carbonization temperature. The size of Ni particle was the biggest at 750 °C. The adsorption of MO into Ni/OMCs followed the Sips adsorption model. More interestingly, a simple equation was obtained and was proved to well fit the desorption behavior of MO on Ni/OMCs. The values for the relative fitted parameters were obtained and the physical meanings of the parameters were well defined.

1. Introduction

Ordered mesoporous carbons have attracted great technological interest due to their remarkable properties such as high specific surface area, narrow pore size distribution, tunable pore structure, large pore volume and high thermal and mechanical stability for the development of drug delivery system, electronic, catalytic, energy storage, adsorption and purification of water [1–9]. Dyes were a kind of toxic environmental pollutants, which had become one of the most serious water pollutants. In view of the dye stability to light and oxidizing agents as well as resistance to biodegradation, the adsorption could be used as an effective technique in the treatment of dye-containing wastewaters [8,10–13]. Mesoporous carbons, due to large pore sizes, provided more advantages in bulky dye molecular adsorption than commercial activated carbon with small micropore sizes [9,14–18]. However, carbon powders were notoriously difficult to be separated from solutions. The conventional approach normally involved a filtration or centrifugation procedure, which was rather complex [19].

Magnetic mesoporous carbons containing Ni, Fe, Co or alloyed magnetic nanoparticles, provided an alternative opportunity for the separation. Magnetic Ni-containing ordered mesoporous carbons (Ni/OMCs) using silica-template synthesis were widely used due to their high specific surface areas and pore volumes, the structural ordering of pores, high stability, and facile functionalization [20,21]. Recently, Wang et al. [22] synthesized Fe–Ni magnetic carbon materials by using a simpler method.

However, solvents that needed for dissolving carbon precursor or magnetic source were the drawbacks for these synthesis routes. Consequently, an easy and simple synthesis procedure for magnetic Ni/OMCs was in urgent demand for practical applications. Herein, we successfully present a simple and novel route to synthesize magnetic Ni/OMCs without using a solvent for dissolving carbon precursor or magnetic source. Carbon precursor (furfuryl alcohol, FA) and nickel source ($Ni(NO_3)_2$) were introduced simultaneously into the silica template in one step. The effects of $Ni(NO_3)_2$ loading and carbonization temperature on pore structures parameters and magnetic properties of these Ni/OMCs were intensively investigated. Methylene orange (MO, C.I. number 13025) was a typical water-soluble anionic dye with molecular weight of 327.3 g/mol (Fig. 1). By use of MO as a model pollutant, the MO adsorption and desorption properties of Ni/OMCs were studied. More interestingly, we obtained a simple equation, which was proved to well fit the desorption behavior of MO on Ni/OMCs. The values for relative fitted parameters were obtained and the physical meanings of the parameters were well defined.

* Corresponding author. Tel.: +86 2039352129; fax: +86 2039352129.
E-mail address: x_f_wang@163.com (X. Wang).

0304-3894/$ – see front matter © 2012 Elsevier B.V. All rights reserved.
doi:10.1016/j.jhazmat.2012.02.011

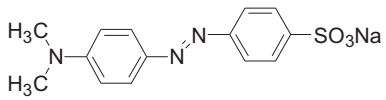

Fig. 1. The structural formula of methylene orange ($C_{14}H_{14}N_3O_3SNa$).

2. Materials and methods

2.1. Synthesis of magnetic carbon materials

Incipient-wetness impregnation method was employed to introduce simultaneously carbon precursor (FA) and magnetic source ($Ni(NO_3)_2{\cdot}6H_2O$) into the SBA-15 templates. Typically, 1.0 mmol of $Ni(NO_3)_2{\cdot}6H_2O$ was dissolved in 2 ml of FA solution. SBA-15 was impregnated with the above solution at room temperature. The mixture thus prepared was heated at 80 °C for 12 h under vacuum for the polymerization of FA and then at 150 °C for 6 h. After cooling to room temperature, the sample was heated to 300 °C (1 °C/min), then to 900 °C (2 °C/min) for 3 h under flowing N_2 atmosphere (200 ml/min) in a tubular furnace (KTL-1400). The silica templates were removed by boiling the materials in 1 M NaOH solution dissolved in 1:1 (v:v) mixtures of water and ethanol for more than 1 h twice. The obtained black powders were filtered, washed with water and dried under vacuum at 60 °C for 24 h. The obtained sample was denoted as Ni-C-1.0-900. The same procedures were carried out for the preparation of sample Ni-C-0.5-900 and Ni-C-1.5-900, except that the amounts of $Ni(NO_3)_2{\cdot}6H_2O$ were 0.5 and 1.5 mmol for Ni-C-0.5-900 and Ni-C-1.5-900. The similar samples were denoted as Ni-C-1.0-600 and Ni-C-1.0-750, where 600 and 750 referred to carbonization temperature (°C). SBA-15 template used in this study was synthesized according to Zhao and co-workers [23].

2.2. Adsorption and desorption of MO

In the adsorption experiment, a typical process was as follows: different masses of carbon materials were added into 25 ml of MO solution with initial concentration of 35 mg/l. The resulting mixture was continuously stirred in a closed batch at 30 °C until equilibrium was reached. This was done by monitoring the MO concentration using a UV–vis spectrophotometer at a wavelength of 464 nm. The adsorbed amount of MO onto the samples was determined according to the change of concentration before and after adsorption. In the desorption studies, 20 mg of the loaded materials were immersed into 50 ml of ethanol at 30 °C under stirring (100 rpm). 3 ml of medium was removed at given time intervals and analyzed by UV–visible spectroscopy at a wavelength of 418 nm. The volume removed was replaced with the same volume and temperature of ethanol.

In the fixed bed column studies, the inner diameter of the adsorption column was 1 cm and the filled bed height was 5 cm keeping the flow rate and initial MO concentration as constant at 2 ml/min and 35 mg/l, respectively.

2.3. Characterization

The X-ray diffraction (XRD) patterns were recorded on a multi purpose diffractometer (PANanalytical. Inc. X'Pert Pro., MPD) with Cu KR radiation (0.1540 nm), using an operating voltage of 40 kV and 40 mA, 0.017° step size, and 4.96 s step time. Nitrogen adsorption isotherms were measured with a volumetric adsorption analyzer (Micromeritics Tristar 3020) at −196 °C. The samples were degassed at 150 °C for 5 h prior to the measurements. The specific surface areas of the samples were calculated by using the Brunauer–Emmett–Teller (BET) method. The pore size

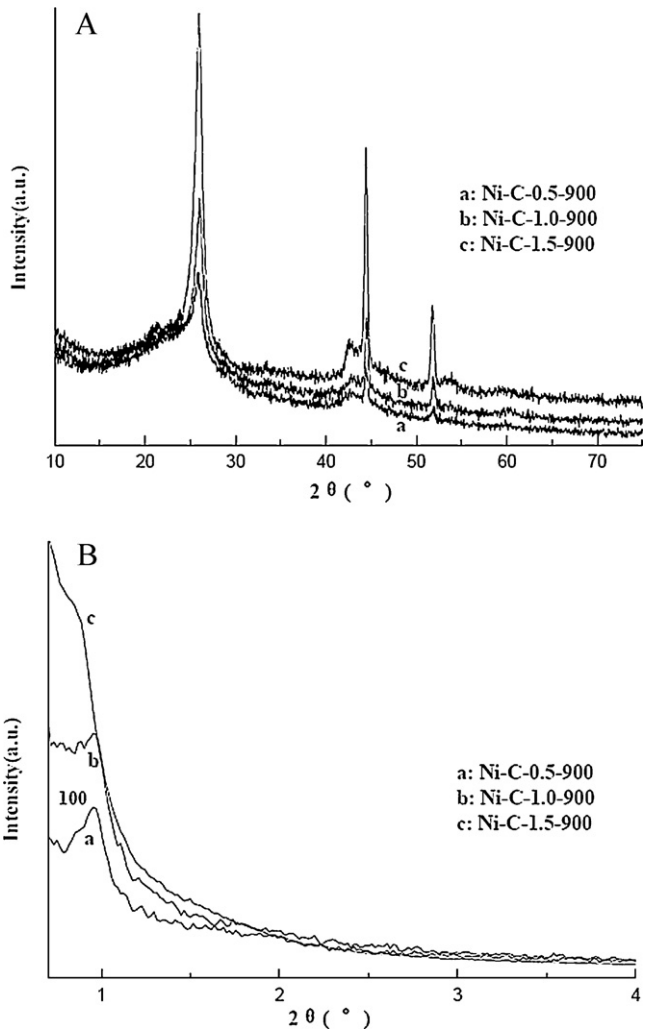

Fig. 2. Wide-angle (A) and small-angle (B) XRD patterns for the Ni/OMCs with different Ni contents ((a) Ni-C-0.5-900; (b) Ni-C-1.0-900; (c) Ni-C-1.5-900).

distributions were derived from the adsorption branches of isotherms by using the Barett–Joyner–Halenda (BJH) model, and the total pore volumes (V_t) were estimated from the adsorbed amount at a relative pressure P/P_0 of 0.99. Transmission electron microscopy (TEM) was performed on a JEOL 2011 microscope operated at 200 kV. The UV–visible absorption spectra values were measured on a U-3010 spectrophotometer. The field-dependent magnetization curve of the materials was measured in a magnetic field of ±20 kOe at 27 °C using physical property measurement system (PPMS-9).

3. Results and discussion

Fig. 2 showed the wide- and small-angle XRD patterns for Ni-C-0.5-900, Ni-C-1.0-900, Ni-C-1.5-900, respectively. The wide-angle XRD patterns (Fig. 2A) exhibited three well resolved diffraction peaks at $2\theta = 26.2$, 44.5, 51.8° and a weak diffraction peak at 42.5° for all samples prepared at 900 °C. 26.2° and 42.5° could be indexed to the (0 0 2) and (1 0 0) diffraction peak of the graphite structure (JCPDS card no. 130148). The interlayer spacing value (d-spacing) of the (0 0 2) plane was 0.344 nm, a little bigger than the value (0.335 nm) for graphite [24], suggesting that the materials were well graphitized by the nickel nanoparticles during carbonization at 900 °C, which was much lower than graphitized temperature (at 2400 °C) of pure OMC [25]. The lower graphitized temperature of

Ni/OMCs was due to the existence of the Ni nanoparticles. It was well known that the nanosized transition metals such as Ni, Fe, Co, Mn could accelerate the development of graphitic structure of carbon when they were heat-treated together with carbon materials in inert gas atmosphere [26–28].

44.5° and 51.8° could be assigned to the (1 1 1) and (2 0 0) characteristic reflections from face centered cubic Ni (JCPDS card no. 040850), while no nickel oxide was detected. The formation of Ni was probably realized through reduction reaction of nickel oxide or nickel nitrate during the carbonization pyrolysis [9]. The magnetic nanoparticle size was estimated by using the Scherrer equation of diffraction peak widths for (1 1 1) peak of Ni. The average crystal sizes of Ni were 26.1, 37.3 and 43.6 nm for Ni-C-0.5-900, Ni-C-1.0-900 and Ni-C-1.5-900, respectively, increasing with the increase of $Ni(NO_3)_2$ loading amount, which might contribute to the aggregation and growth of Ni nanoparticles with neighbors to form bigger ones at higher $Ni(NO_3)_2$ loading amount.

The low-angle XRD peaks (Fig. 2B) became less visible with an increase of $Ni(NO_3)_2$ amounts, showing a gradual loss of mesoporous structural order. Ni-C-0.5-900 and Ni-C-1.0-900 exhibited well-resolved diffraction peaks, confirming a well-ordered mesoporous structure of the materials. Ni-C-1.5-900 exhibited poorly-resolved scattering peaks, indicating that the ordering of mesoporous structure had been partially deteriorated with the increase of $Ni(NO_3)_2$ loading amount. The decrease of carbon matrix and larger Ni particles affected the replication integrality of Ni/OMCs from the ordered SBA-15 templates.

Furthermore, more carbon was consumed owing to the reduction reaction of nickel oxide or nickel nitrate with the increase of $Ni(NO_3)_2$ loading amount, also leading to partial loss of the ordering and the distortion of the porous channel.

Fig. 3 showed the wide and small angle XRD patterns at different carbonization temperatures. The average particles sizes of Ni were 25.3, 43.1 and 37.3 nm for Ni-C-1.0-600, Ni-C-1.0-750 and Ni-C-1.0-900, respectively. Remarkably, Ni-C-1.0-900 exhibited a strong XRD peak at 2θ around 26.2° (Fig. 3A) after being heated up to 900 °C, showing the formation of a highly graphitic carbon. It was in favor of the aggregation and growth of the metal nanoparticles at elevated temperatures (such as from 600 to 750 °C). The particle sizes carbonized at 900 °C were smaller than the sizes at 750 °C. This was probably due to the presence of highly graphitic carbon at 900 °C according to the wide-angle XRD results. The presence of graphitic domains limited the migration, aggregation and growth of Ni nanoparticles, according to these studies [9,21].

The low-angle XRD patterns of the Ni/OMCs at different temperatures were presented in Fig. 3B.The (1 0 0) peaks of carbon materials had a slight shift from 2θ value of 0.88, 0.92, to 0.98 with the increase of carbonization temperatures, implying the increasing of structural shrinkage due to higher carbonization temperatures. The Ni-C-1.0-900 sample showed intense (1 0 0) diffraction peaks, which indicated that the sample possessed well-ordered mesoporous structure. However, weak (1 0 0) peaks were observed in the Ni-C-1.0-600 and Ni-C-1.0-750 samples. Lower carbonization temperature did not facilitate the complete carbonization of the furfuryl alcohol polymer, which could not form a sufficiently rigid skeleton to resist the structural shrinkage, and correspondingly the decrease of the structural ordering. In addition, the bigger Ni particle sizes at 750 °C also contributed to the decrease of the ordering for Ni-C-1.0-750. This phenomenon was in good agreement with the TEM results (Fig. 4b, d and e).

Fig. 4 showed the TEM images for all samples. The ordered arrangement of mesopores was clearly observed for Ni-C-0.5-900 (Fig. 4a) and Ni-C-1.0-900 (Fig. 4b), giving evidence for the presence of ordered hexagonal mesoporous structure. While Ni-C-1.5-900 (Fig. 4c) showed some less ordered arrays, which was consistent with the results of XRD analysis. The dark spots were observed for

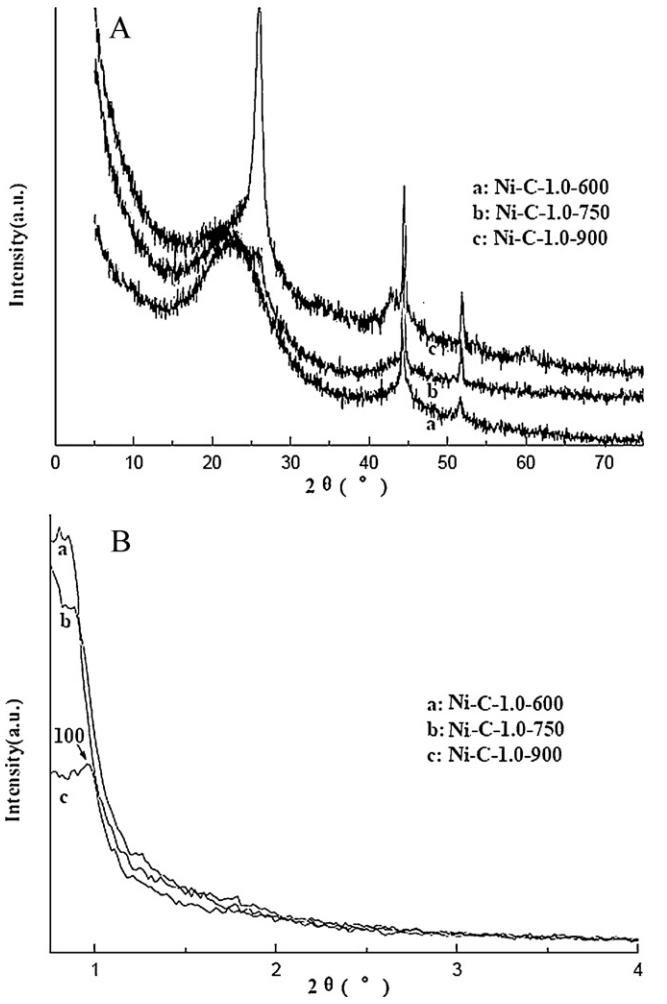

Fig. 3. Wide-angle (A) and small-angle (B) XRD patterns for the Ni-OMCs at different carbonization temperatures.

Ni nanoparticles, which were well dispersed into the carbon matrix and no bulk aggregates could be found on the outside surface of the mesoporous carbons. The TEM results indicated that the materials were stable for application in separation.

N_2 sorption isotherms and pore size distributions of Ni/OMCs were presented in Fig. 5. N_2 sorption isotherms of magnetic mesoporous carbons exhibited type IV curves with an obvious capillary condensation at a relative pressure P/P_0 0.2–0.4 (Fig. 5A and C), indicating a uniform mesoporosity with a narrow pore size distribution (Fig. 5B and D). The calculated parameters were listed in Table 1. The specific surface area and the total pore volumes decreased with the increasing usage of $Ni(NO_3)_2$, which might arise from the high density of Ni and the destruction of ordered mesoporous structure. The mean pore diameters for Ni-C-0.5-900, Ni-C-1.0-900 and Ni-C-1.5-900 exhibited an increasing tendency from 3.1, 4.5 to 5.3 nm. This was probably ascribed to the consumption of carbon during the reduction process of nickel oxide/nickel nitrate to Ni by surrounding carbon.

The specific surface area and the total pore volumes decreased with the increasing of the carbonization temperature, which might be due to the increased structural shrinkage with the temperature increasing according to low-angle XRD results.

The magnetization curves for the Ni-C-0.5-900, Ni-C-1.0-900 and Ni-C-1.5-900 (Fig. 6A) presented a small hysteresis loop. The corresponding saturation magnetization strengths were 0.7, 1.9 and 3.6 emu/g, increasing with the increase of $Ni(NO_3)_2$ usage. This

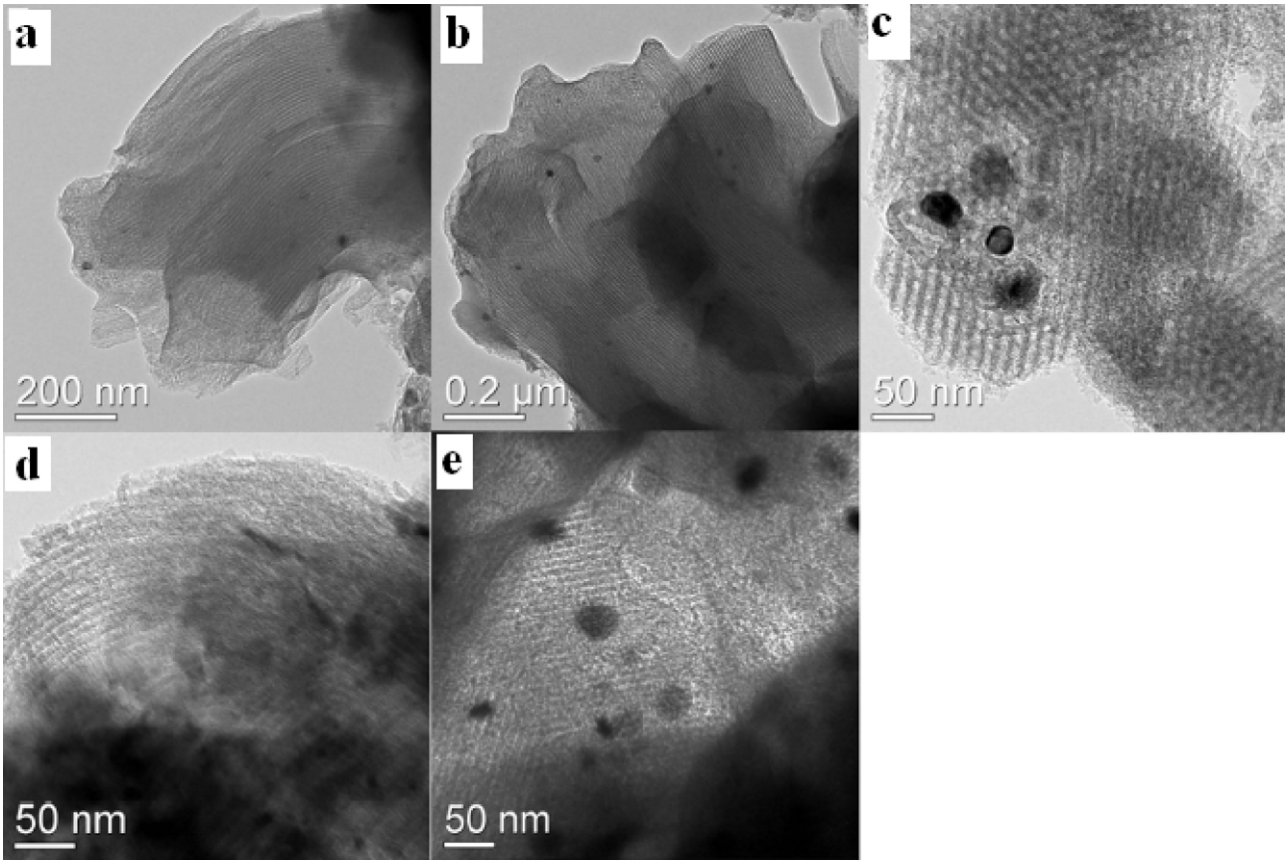

Fig. 4. The TEM images for the Ni-OMCs ((a) Ni-C-0.5-900; (b) Ni-C-1.0-900; (c) Ni-C-1.5-900; (d) Ni-C-1.0-600; (e) Ni-C-1.0-750).

Table 1
The structural parameters for Ni/OMCs and the fitted data by Sips adsorption isotherm equation.

Sample	S_{BET} (m^2/g)	V_t (cm^3/g)	D_{pore} (nm)	q_m (mg/g)	K (l/mg)	m
Ni-C-0.5-900	796	0.40	3.1	107.1	0.71	0.60
Ni-C-1.0-900	479	0.34	4.5	94.8	0.99	0.73
Ni-C-1.5-900	347	0.31	5.3	90.6	0.89	0.88
Ni-C-1.0-600	686	0.45	5.2			
Ni-C-1.0-750	497	0.41	4.7			

could be ascribed to the growth in sizes of magnetic nanoparticles with the increase of $Ni(NO_3)_2$ usage. The values of the saturation magnetization strengths were much lower than that of the bulk Ni (51.3 emu/g) [29], mainly due to the much smaller Ni particle size and inclusion of the Ni particles inside the non-magnetic carbon frameworks. The near-zero coercive force and remanence magnetization indicated that the samples exhibited soft ferromagnetic characteristics desirable for the application in adsorption and separation under an external magnetic field.

The magnetic separability of the magnetic Ni-C-1.0-900 was tested in MO aqueous solution (Fig. 6B). Upon placement of a magnet near the glass bottle, the powder Ni-C-1.0-900 were quickly attracted to the side of the bottle and the colored liquid changes from orange to transparent within a few minutes. Considering their magnetic property, this provided an easy and effective way for the removal of pollutants such as dye in water.

The adsorption equilibrium of MO onto the Ni/OMCs was shown in Fig. 7A. The Sips adsorption isotherm equation [10] was used to fit the adsorption data.

$$q = q_m \frac{(Kc)^m}{1 + (Kc)^m} \quad (1)$$

where, q was the adsorption amount, q_m was the adsorption capacity, K was the equilibrium constant, c was the concentration of MO at equilibrium, and m was the heterogeneity coefficient. The determination coefficient (R^2) was greater than 0.99. The obtained parameters are listed in Table 1.

As seen in Table 1, the adsorption capacity increased with the increase of the specific surface area and pore volume of Ni/OMCs. For Ni-C-0.5-900, q_m was 107 mg/g, whereas 95 and 91 mg/g could be obtained for Ni-C-1.0-900 and Ni-C-1.5-900, respectively. It was well known that the bigger the specific surface area and pore volume, the more chance and space for MO adsorption on Ni/OMCs were, thus leading to the higher adsorption capacity. The heterogeneity coefficient of m values less than 1 indicated a heterogeneous system [30]. Values close to (or exactly) 1 indicated a material with relatively homogenous binding sites. The m decreased with the increase of the specific surface area and pore volume of Ni/OMCs. Also seen in Table 1, the values of the equilibrium constant K did not vary significantly, which implied that the affinity of the Ni/OMCs for MO was very similar.

The adsorption and desorption column dynamic study was shown in Fig. S1. The adsorbent Ni-C-1.0-900 exhibited high adsorption performance at the beginning of adsorption process with the first 650 min (Fig. S1A). The desorption fraction could reach

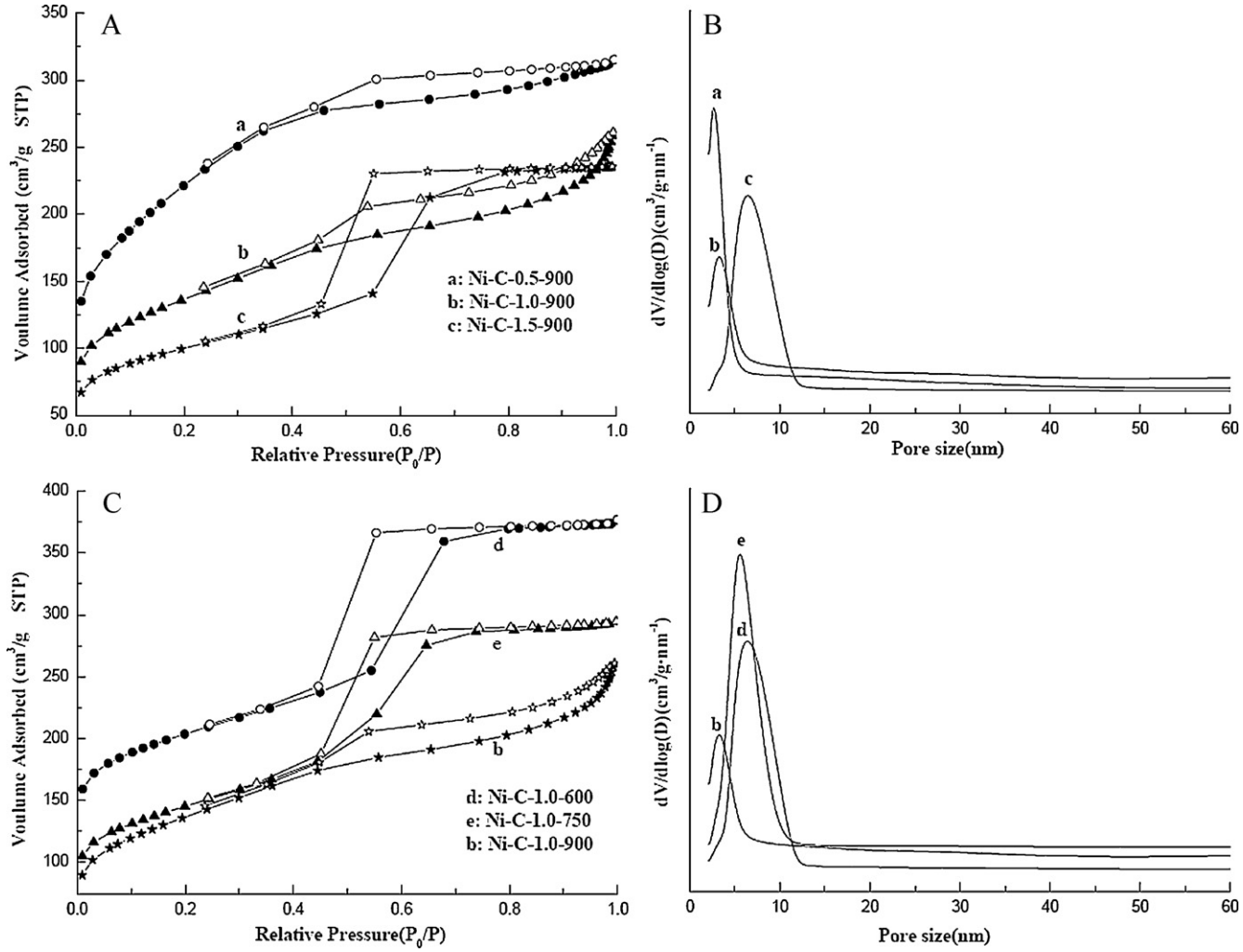

Fig. 5. N_2 sorption isotherms (A,C) and pore size distributions (B,D) for the Ni-OMCs with different Ni contents and at different carbonization temperatures.

up to 90% when the eluting time approached 300 min (Fig. S1B). This could imply that the interaction between the sorbent and MO was weak enough to be broken by ethanol eluent.

Fig. S2 showed the relationship of adsorption amount versus equilibrium concentration at different temperatures (for the adsorption of MO onto Ni-C-1.0-900). The adsorption capacity decreased with increasing temperatures (from 293 to 313 K), which might be indicative of physical adsorption. Thermodynamic parameters as free energy change (ΔG°), enthalpy change (ΔH°) and entropy change (ΔS°) were evaluated using the following equations [31]:

$$\Delta G^\circ = -RT \ln K \quad (2)$$

$$\Delta G^\circ = \Delta H^\circ - T\Delta S^\circ \quad (3)$$

where K denoted the equilibrium constant, R was the gas constant, and T was absolute temperature. Thermodynamic parameters are listed in Table 2. Free energy changes (ΔG°) were all negative, demonstrating that the studied adsorption was a spontaneous process. For the given sample (the adsorption of MO onto Ni-C-1.0-900), the absolute values of ΔG° decreased with increasing temperature. Therefore, higher temperature was favorable for the reverse process of adsorption–desorption. Values for enthalpy changes (ΔH°) were negative and the absolute values were lower than 40 kJ mol^{-1}, which indicated that the adsorption was an exothermic physical process [32].

Negative values of the entropy change (ΔS°) suggested that there was decreased randomness at the solid-solution interface during the adsorption of MO in aqueous solution on Ni/OMCs.

Fig. S3 showed the relationship of adsorption amount versus time at different temperatures. The adsorption amount at different temperatures increased with the increasing of adsorption time and eventually reached equilibrium. The adsorption amount in equilibrium decreased with the increasing of temperatures, due to high temperature in disadvantage for physical adsorption. It was noticeable that the slope of the curves in Fig. S3 increased with the increasing of temperatures in the first 25 min, indicating high temperature increasing adsorption rate. It was well known that increasing the temperature would increase the rate of diffusion of the MO molecules in solution and decrease the viscosity of the solution. So the MO molecules diffused faster into the surface and internal pores of Ni/OMCs in high temperature.

Fig. 7B shows the MO desorption behavior for the three MO-loaded Ni/OMCs. They exhibited a similar desorption relationship. First, a fast release and then a slower desorption were observed.

Interestingly, the desorption rate could be well described by the following equation:

$$V = \frac{df}{dt} = k(a-f)^2 \quad (4)$$

where, f was the desorption fraction of MO, t was time, k was defined as desorption reaction rate constant and a denoted a

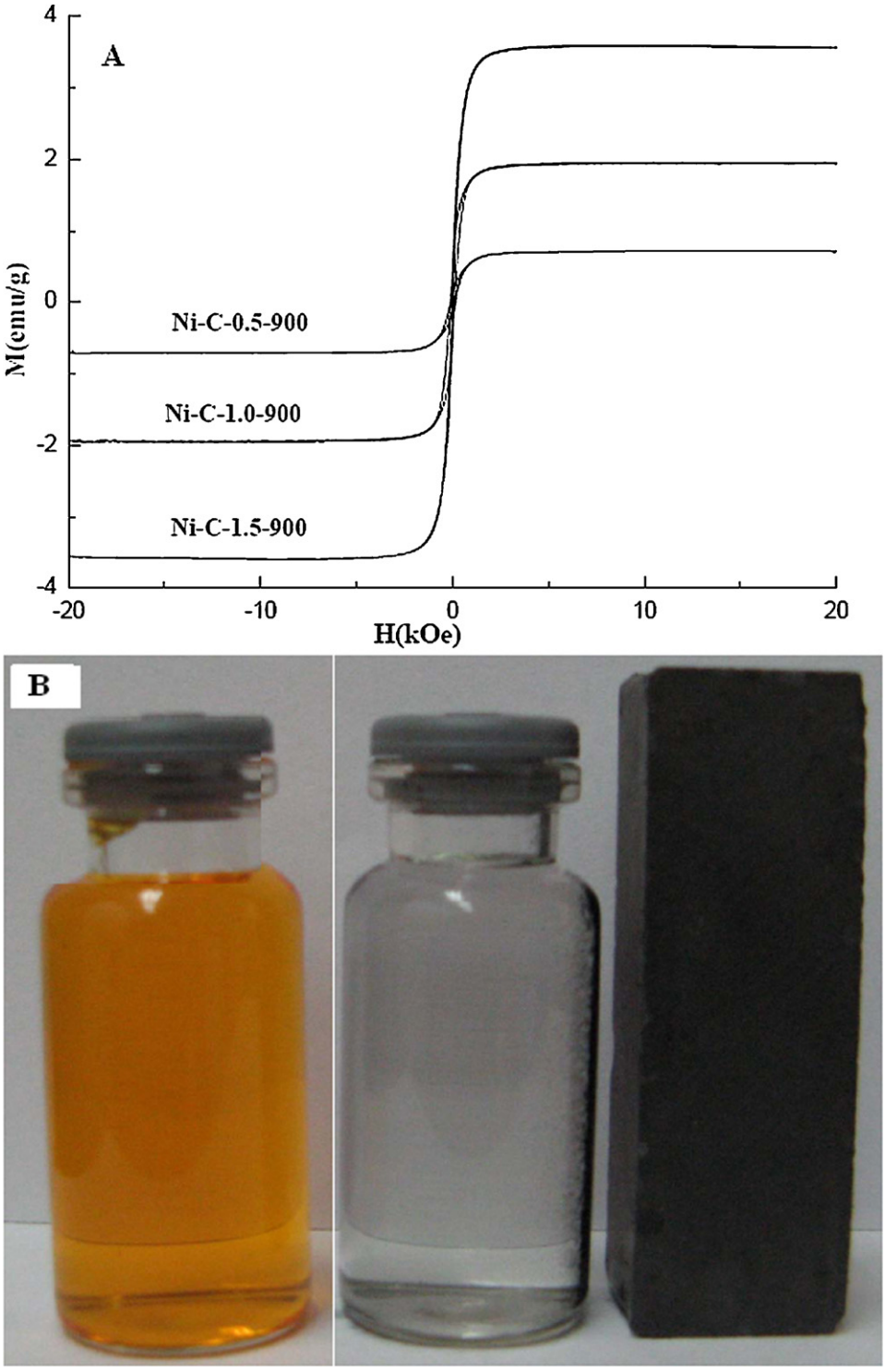

Fig. 6. The magnetization curves (A) for the Ni-OMCs and images of the magnetic separability (B).

Table 2
Thermodynamic parameters for the adsorption of MO on Ni-C-1.0-900.

ΔG° (kJ mol^{-1})			ΔH° (kJ mol^{-1})	ΔS° (J mol^{-1} K^{-1})
293 K	303 K	313 K	−35.87	−13.01
−32.05	−31.96	−31.79		

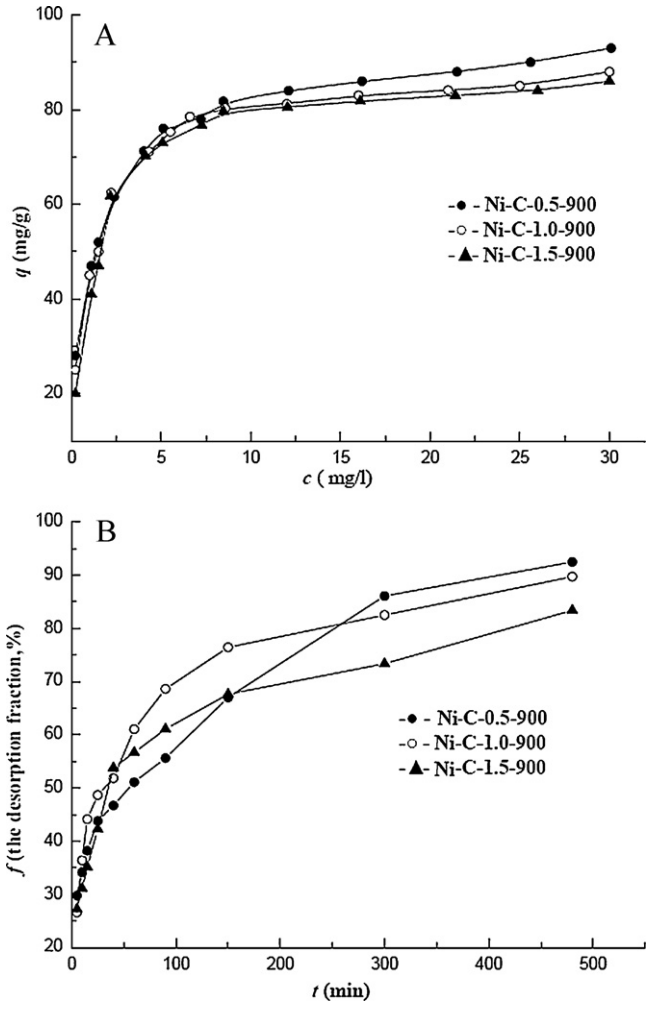

Fig. 7. The adsorption equilibrium (A) and desorption behavior (B) for the Ni-OMCs with different Ni contents.

parameter, the physical meaning of which was defined in the following description. The kinetic equation given for desorption is similar to pseudo-second order kinetic model. It was used for desorption instead of adsorption.

After integration of Eq. (4), we obtain the following equation,

$$f = \frac{ka^2t}{1 + kat} \tag{5}$$

where, when $t \to \infty$, $f = a$ (the fraction of the maximum desorption). Thus the physical meaning of the parameter (a) was obtained.

After transformation of Eq. (5), we could easily obtain:

$$\frac{t}{f} = \frac{1}{ka^2} + \frac{t}{a} \tag{6}$$

A simple linear equation could be obtained and fitted to these data with a correlation coefficient of >0.99. Through the plot of (t/f) versus t, the values of parameter k (0.96, 0.91, 0.85) and a (0.028, 0.045, 0.048) were achieved for Ni-C-0.5-900, Ni-C-1.0-900 and Ni-C-1.5-900, respectively.

The result indicated that the pore size and the ordering of the materials had great influence on the MO desorption rate and the fraction of the maximum desorption. The MO desorption rate increased with the increasing of pore sizes for the carbon materials. Large pore sizes were favorable for desorption of MO molecules from the materials to ethanol solution, which increased the MO desorption rate. The fraction of the maximum desorption decreased with the decreasing of the ordering. The distortion of the ordered channel would hinder the complete desorption of MO molecules.

4. Conclusions

A simple route has been developed to synthesize magnetic Ni/OMCs without using a solvent for dissolving carbon precursor or magnetic source. The nickel nanoparticles were uniformly distributed in the OMCs. The structural parameters and magnetic properties of the Ni/OMCs were dependent on $Ni(NO_3)_2$ loading amount and the carbonization temperature. The materials exhibited soft ferromagnetic characteristics desirable for the application in adsorption and separation. The adsorption of MO onto Ni/OMCs followed the Sips adsorption model. Especially, a simple equation was obtained and was proved to well fit the desorption behavior of MO on Ni/OMCs. The values for relative parameters were obtained and the physical meanings of the parameters were well defined. It was expected that the simple equation could become a common equation to the physical desorption of other molecules in porous materials.

Acknowledgments

The authors acknowledge the financial support from the National Science Foundation of China (no. 50802017) and Higher Education Talents Introducing Fund of Guangdong Province (2011).

Appendix A. Supplementary data

Supplementary data associated with this article can be found, in the online version, at doi:10.1016/j.jhazmat.2012.02.011.

References

[1] Y. Fang, D. Gu, Y. Zou, Z.X. Wu, F.Y. Li, R.C. Che, Y.H. Deng, B. Tu, D.Y. Zhao, A low-concentration hydrothermal synthesis of biocompatible ordered mesoporous carbon nanospheres with tunable and uniform size, Angew. Chem. Int. Ed. 49 (2010) 7987–7991.
[2] Y. Tian, P. Liu, X.F. Wang, H.S. Lin, Adsorption of malachite green from aqueous solutions onto ordered mesoporous carbons, Chem. Eng. J. 171 (2011) 1263–1269.
[3] X.F. Wang, P. Liu, Y. Tian, Ordered mesoporous carbons for ibuprofen drug loading and release behavior, Microporous Mesoporous Mater. 142 (2011) 334–340.
[4] X.Q. Wang, S. Dai, A simple method to ordered mesoporous carbons containing nickel nanoparticles, Adsorption 15 (2009) 138–144.
[5] X.F. Wang, P. Liu, Y. Tian, Preparation and drug release behavior of temperature-responsive mesoporous carbons, J. Solid State Chem. 184 (2011) 571–1575.
[6] Y.F. Zhu, E. Kockrick, S. Kaskel, T. Ikoma, N. Hanagata, Nanocasting route to ordered mesoporous carbon with FePt nanoparticles and its phenol adsorption property, J. Phys. Chem. C 113 (2009) 5998–6002.
[7] P.F. Fulvio, M. Jaroniec, C.D. Liang, S. Dai, Polypyrrole-based nitrogen-doped carbon replicas of SBA-15 and SBA-16 containing magnetic, J. Phys. Chem. C 112 (2008) 13126–13133.
[8] Z.H. Sun, L.F. Wang, P.P. Liu, S.C. Wang, B. Sun, D.Z. Jiang, F.S. Xiao, Magnetically motive porous sphere composite and its excellent properties for the removal of pollutants in water by adsorption and desorption cycles, Adv. Mater. 15 (2006) 1968–1971.
[9] Y.P. Zhai, Y.Q. Dou, X.X. Liu, S.S. Park, C.S. Ha, D.Y. Zhao, Soft-template synthesis of ordered mesoporous carbon/nanoparticle nickel composites with a high surface area, Carbon 49 (2011) 545–555.
[10] A. Derylo-Marczewska, A.W. Marczewski, Sz. Winter, D. Sternik, Studies of adsorption equilibrium and kinetics in the systems: aqueous solution of dyes – mesoporous carbons, Appl. Surf. Sci. 256 (2010) 5164–5170.
[11] V.K. Gupta, Suhas, Application of low cost adsorbents for dye removal – a review, J. Environ. Manage. 90 (2009) 2313–2342.
[12] V.K. Gupta, B. Gupta, A. Rastogi, S. Agarwal, A. Nayak, A comparative investigation on adsorption performances of mesoporous activated carbon prepared from waste rubber tire and activated carbon for a hazardous azo dye – Acid Blue 113, J. Hazard. Mater. 186 (2011) 891–901.
[13] B.C. Kim, J. Lee, W. Um, J. Kim, J. Joo, J.H. Lee, J.H. Kwak, J.H. Kim, C. Lee, H. Lee, R.S. Addleman, T. Hyeon, M.B. Gu, J. Kim, Magnetic mesoporous materials for removal of environmental wastes, J. Hazard. Mater. 192 (2011) 1140–1147.
[14] X. Yuan, S.P. Zhuo, W. Xing, H.Y. Cui, X.D. Dai, X.M. Liu, Z.F. Yan, Aqueous dye adsorption on ordered mesoporous carbons, J. Colloid Interface Sci. 310 (2007) 83–89.

[15] S.J. Han, K. Sohn, T. Hyeon, Fabrication of new nanoporous carbons through silica templates and their application to the adsorption of bulky dyes, Chem. Mater. 12 (2000) 3337–3341.
[16] P. Ariyadejwanich, W. Tanthapanichakoon, Preparation and characterization of mesoporous activated carbon from waste tires, Carbon 41 (2003) 157–164.
[17] W. Tanthapanichakoon, P. Ariyadejwanich, P. Japthong, K. Nakagawa, S.R. Mukai, H. Tamon, Adsorption–desorption characteristics of phenol and reactive dyes from aqueous solution on mesoporous activated carbon prepared from waste tires, Water Res. 39 (2005) 1347–1353.
[18] Y.R. Lin, H. Teng, Mesoporous carbons from waste tire char and their application in wastewater discoloration, Microporous Mesoporous Mater. 54 (2002) 167–174.
[19] Y.P. Zhai, Y.Q. Dou, X.X. Liu, B. Tu, D.Y. Zhao, One-pot synthesis of magnetically separable ordered mesoporous carbon, J. Mater. Chem. 19 (2009) 3292–3300.
[20] I.S. Park, M. Choi, T.W. Kim, R. Ryoo, Synthesis of magnetically separable ordered mesoporous carbons using furfuryl alcohol and cobalt nitrate in a silica template, J. Mater. Chem. 16 (2006) 3409–3416.
[21] P.F. Fulvio, C.D. Liang, S. Dai, M. Jaroniec, Mesoporous carbon materials with ultra-thin pore walls and highly dispersed nickel nanoparticles, Eur. J. Inorg. Chem. (2009) 605–612.
[22] Z.L. Wang, X.J. Liu, M.F. Lv, J. Meng, Simple synthesis of magnetic mesoporous FeNi/carbon composites with a large capacity for the immobilization of biomolecules, Carbon 48 (2010) 3182–3189.
[23] Y. Wan, X.F. Qian, N.Q. Jia, Z.Y. Wang, H.X. Li, D.Y. Zhao, Direct triblock-copolymer-templating synthesis of highly ordered fluorinated mesoporous carbon, Chem. Mater. 20 (2008) 1012–1018.
[24] T. Hiraoka, T. Kawakubo, J. Kimura, R. Taniguchi, A. Okamoto, T. Okazaki, Selective synthesis of double-wall carbon nanotubes by CCVD of acetylene using zeolite supports, Chem. Phys. Lett. 382 (2003) 679–685.
[25] X. Wang, C. Liang, S. Dai, Facial synthesis of ordered mesoporous carbons with high thermal stability by self-assembly of resorcinol-formaldehyde and block copolymers under highly acidic conditions, Langmuir 24 (2008) 7500–7505.
[26] J.Y. Yao, L.X. Li, H.H. Song, C.Y. Liu, X.H. Chen, Synthesis of magnetically separable ordered mesoporous carbons from F127/$[Ni(H_2O)_6](NO_3)_2$/resorcinol–formaldehyde composites, Carbon 47 (2009) 436–444.
[27] W. Weisweiler, N. Subramanian, B. Terwiesch, Catalytic influence of metal melts on the graphitization of monolithic glasslike carbon, Carbon 9 (1971) 755–758.
[28] J.S. Li, J. Gu, H.J. Li, Y. Liang, Y.X. Hao, X.Y. Sun, Synthesis of highly ordered Fe-containing mesoporous carbon materials using soft templating routes, Microporous Mesoporous Mater. 128 (2010) 144–149.
[29] P.Z. Si, Z.D. Zhang, D.Y. Geng, C.Y. You, X.G. Zhao, W.S. Zhang, Synthesis and characteristics of carbon-coated iron and Nickel nanocapsules produced by arc discharge in ethanol vapor, Carbon 41 (2003) 247–251.
[30] S.K. Papageorgious, F.K. Katsaros, E.P. Kouvelos, J.W. Nolan, H. Le Deit, N.K. Kanellopoulos, Heavy metal sorption by calcium alginate beads from Laminaria digitata, J. Hazard. Mater. 137 (2006) 1765–1772.
[31] N. Mohammadi, H. Khani, V.K. Gupa, E. Amereh, S. Agarwal, Adsorption process of methyl orange dye onto mesoporous carbon material-kinetic and thermodynamic studies, J. Colloid Interface Sci. 362 (2011) 457–462.
[32] M. Kara, H. Yuzer, E. Sabah, M.S. Celik, Adsorption of cobalt from aqueous solutions onto sepiolite, Water Res. 37 (2003) 224–232.